Eur. Phys. J. D **2**, 63–73 (1998)

THE EUROPEAN PHYSICAL JOURNAL D

Predictions of geometrical structures and ionization potentials for small barium clusters Ba_n

V. Boutou[1], A.R. Allouche[1], F. Spiegelmann[2], J. Chevaleyre[1], and M. Aubert Frécon[1,a]

[1] Laboratoire de Spectrométrie Ionique et Moléculaire[b], Université Claude Bernard Lyon I, Bâtiment 205, 43 Bd. du 11 Novembre 1918, 69622 Villeurbanne Cedex, France
[2] Laboratoire de Physique Quantique[c], IRSAMC, Université Paul Sabatier, 118 Route de Narbonne, 31062 Toulouse Cedex, France

Received: 14 May 1997 / Received in final form: 2 February 1998 / Accepted: 27 February 1998

Abstract. The geometrical structure of ground state Ba_n clusters ($n = 2-14$) has been predicted from various types of calculations including two *ab initio* approaches used for the smaller sizes namely HF+MP2($n = 2-6$), DFT (LSDA)($n = 2-6$, 9) and one model approach HF+pairwise dispersion used for all sizes investigated here. The lowest energy configurations as well as some isomers have been investigated. The sizes $n = 4$, 7 and 13 are predicted to be the relatively more stable ones and they correspond to the three compact structures: the tetrahedron, the pentagonal bipyramid and the icosahedron. The growth behavior from Ba_7 to Ba_{13} appears to be characterized by the addition of atoms around a pentagonal bipyramid leading to the icosahedral structure of Ba_{13} which is consistent with the observed size-distribution of barium clusters. Values for vertical ionization potentials calculated for $n = 2-5$ at the CI level are seen to be in quite good agreement with recent measures.

PACS. 36.40.-c Atomic and molecular clusters – 36.40.Mr Spectroscopy and geometrical structure of clusters

1 Introduction

A general goal in the studies of metallic clusters is the understanding of transition from molecular to metallic character. In the particular case of alkaline-earth metallic clusters, this evolution starts from the dimer structure which is more or less governed by Van der Waals forces, depending on the metal position in the periodic table. The first observation of barium clusters produced by inert-gas condensation techniques, has been reported by Rayane *et al.* [1]. They suggested that the observed size distribution with large peaks at $n = 13$, 19, 23, 26, 29, 32 could be interpreted by icosahedral close-packing structures. More recently Boutou *et al.* [2] have determined the photoionization efficiency cross sections of small homogeneous barium clusters, produced by a laser vaporization source.

A knowledge of the geometrical structures of small size clusters is crucial to interpret experimental observations. Such information can be provided by theoretical calculations but not directly deduced from experiment. Furthermore, the knowledge of the evolution of cluster properties such as binding energies and ionization potentials (IP's) *versus* cluster size may provide insight into the electronic structure and the binding nature of clusters.

Theoretical studies on Ba clusters are scarce. We knew only two works, one based on the Jellium model [3] and the other on the cylindrically averaged pseudopotential scheme (CAPS) [4]. Predictions of the ionization potential for Ba_n ($n = 2-5$) provided by the jellium model [3] are seen to be rather far from our recent experimental determinations [2]. As far as Ba_{13} is concerned no previous results have been reported for its lowest-energy structure. It should be noted that the most stable configurations calculated for isovalent clusters were not found to be icosahedral for Be_{13} [5] and for Mg_{13} [6,7].

With the aim to help in interpreting the more recent experimental data, we have undertaken a theoretical study of the low-energy lying configurations of Ba_n clusters together with their binding energies and their ionization potentials.

We present various calculations including *ab initio* and model approaches to determine the energy of barium clusters. Those approaches are described in Section 2 together with the optimization procedure. Results are presented and discussed in Section 3 comparatively with available experimental data.

2 Computational techniques

Barium clusters in their ground state are investigated here in a three-dimensional approach by means of several

[a] e-mail: `frecon@in2p3.fr`
[b] UMR 5579 du CNRS
[c] UMR 5626 du CNRS

quantum chemical methods recalled shortly and also through a model based on the addition of two-body dispersion terms to the Hartree-Fock energy. Regarding our limited computational facilities, in the present studies of barium clusters, the barium atoms are described through a two-electron semi-empirical pseudopotential replacing the core, taken from Fuentealba *et al.* [8]

$$V = -\frac{Z}{r} + \sum_{l=0}^{2} B_l \exp(-\beta_l r^2) P_l \qquad (1)$$

where Z is the core charge and

$$P_l = \sum_m |lm><lm|$$

is the projection operator on angular symmetry l. The parameters B_l and β_l ($l = 0, 1, 2$) are available in reference [8] for barium, and such that V (Eq. (1)) reproduces the averaged of the Dirac-Fock valence orbital energy. Thus the pseudopotential used includes some averaged relativistic effects, namely the Darwin and mass terms, spin-orbit coupling excepted which is not expected to play a large role as far as only s orbitals of Barium are concerned (ground state).

2.1 Ab-initio calculations

Among various ab initio methods that can be used to investigate structures for Ba_n, CI calculations would provide the best accuracy. Nevertheless they have not been performed for all the sizes of Ba_n investigated here, due to computational capabilities. Methods based on density functional formalism provide results at more reasonable costs, and then they have been used for larger sizes than CI approaches, nevertheless their accuracy is quite dependent on the functional form used. For the smaller clusters ($n = 2-6$), two types of calculations have been performed. One is based on HF calculations followed by second-order Moller-Plesset perturbation theory MP2 and the other is based on the local spin density approximation (LSDA) in the density functional framework. Calculations at the MP2 level have been performed using the CIPSI (Configuration Interaction by Perturbation of a multiconfiguration wave function Selected Interactively) package [9] of the Laboratoire de Physique Quantique-Toulouse-France(LPQT), and LSDA calculations have been performed with the Gaussian 94 package [10].

The LSDA calculations are assumed here to provide in a satisfactory way, relative values for the energy of different geometrical configurations for a given size and then to predict the correct lowest-energy configuration. Nevertheless, in order to predict reliable ionization potentials we have achieved more sophisticated treatment of the electronic correlation. Namely QCISD(T) calculations *via* the Gaussian 94 package have been performed, for the energies of the Ba_n and of the ionic Ba_n^+ clusters ($n = 2-5$) for geometries previously determined from LSDA calculations. For these small sizes we have also calculated electronic wavefunctions and densities with the three-class iterative MRCI algorithm CIPSI [9]. The wavefunction results from the diagonalization of the larger MRCI subspace M selected from the perturbation of the variational zeroth-order wavefunction in a smaller one S. Subspace S is itself built from a Complete Active Space (CAS) calculation including all the occupied plus the first virtual MO's. Subspace M includes all the determinants, the contributions of which in the first-order wavefunction are larger than a threshold $\eta_M > 0.001$.

A Gaussian basis set (4s3p2d/3s1p1d)(labelled set A) has been used for the MP2 and the LSDA calculations while a larger basis set (5s3p2d/4s3p2d) (labelled set B) has been used in the CIPSI calculations of the electronic densities. Both sets A and B are displayed in Table 1.

Table 1. Atomic Gaussian basis sets A and B.

type of orbital	set A		set B	
	α_i	C_i	α_i	C_i
s	0.693	0.06222	0.603	0.06222
	0.2079	−0.47842	0.2079	−0.47842
	0.0693	1.	0.0693	1.
	0.03465	1.	0.03465	1.
			0.015	1.
p	0.2079	−0.07391	0.2079	1.
	0.0693	0.04464	0.0693	1.
	0.03465	0.98806	0.03465	1.
d	0.693	0.13204	0.693	1.
	0.10395	0.95868	0.10395	1.

2.2 Model calculations

Due to computational capability constraints, we have not performed purely quantum chemical calculations for the largest clusters Ba_n investigated here ($n = 7-8$, $10-14$). Then we propose a model in which the correlation contribution is built up from that of the dimer ground state. The ground state of Ba_2 calculated accurately [11] through a relativistic ten-electron pseudopotential, a core polarization potential including some core effects and CI calculations for the four valence electrons, is weakly bound ($D_e = 0.202$ eV) at rather large internuclear distance ($9.2a_0$). For such weakly bound systems, the interaction energy can be approximated by the sum of the Hartree-Fock energy and the interatomic correlation energy which reduces to the dispersion contribution at large internuclear distance [12]. Then the potential energy curve of Ba_2 may be described by the sum of the Hartree-Fock energy and the long-range dispersion terms varying as R^{-2n}

$$E(Ba_2) = E_{HF}(Ba_2) - \sum_{n=3} \frac{C_{2n} f_{2n}(R)}{R^{2n}} \qquad (2)$$

where R is the interatomic distance, the C_{2n} are the usual expansion coefficients of the dispersion energy in the multipolar approximation while the $f_{2n}(R)$ are damping functions which take some account of the atomic overlap.

In the present calculations we have only considered the first term $\frac{C_6}{R^6}$ and we have used the parameterized form of Tang *et al.* [13] for $f_6(R)$

$$f_6(R) = 1 - \exp(-bR) \sum_{k=0}^{6} \frac{(bR)^k}{k!} \qquad (3)$$

where b has been treated as an adjustable parameter. To the best of our knowledge, no actual accurate value exists in the literature for the C_6 expansion coefficient of Ba_2 so that it has also been treated as an adjustable parameter. From our previous values for the Ba_2 energy [11] and using a reduced basis set containing only the s orbitals of set A for the evaluation of the Hartree-Fock part, the following fitted values have been obtained for the two adjustable parameters $b = 0.83806\ a_0^{-1}$ and $C_6 = 15477.8\ a_0^6$ Hartree. Note that for Ba_2, estimates of the C_6 coefficient are quite different when obtained from the London formula $C_6 = \frac{3}{4} I_{Ba} \alpha_{Ba}^2$ ($\approx 10300\ a_0^6$ Hartree) or from the Slater and Kirkwood formula [14] $C_6 = 3(\frac{\alpha_{Ba}}{2})^{\frac{3}{2}}$ ($\approx 4700\ a_0^6$ Hartree), α_{Ba} is the dipolar static polarisability and I_{Ba} the ionization potential. The larger effective value presently deduced may be considered as taking some account of higher dispersion terms through the fit. This model provides a dissociation energy of 0.16 eV, slightly less than the CI value.

Then for a cluster Ba_n, the energy is calculated from the following expression,

$$E(Ba_n) = E_{HF}(Ba_n) - \sum_{i<j} \frac{C_6 f_6(R_{ij})}{R_{ij}^6} \qquad (4)$$

where R_{ij} are the interatomic distances. This HF + dispersion energy-model is very usual when calculating Van der Waals molecules, as a matter of fact it is known that weak dispersion forces are always very tedious to obtain in *ab initio* calculations. This model is more sophisticated than a pure additive-pair model, since the Hartree-Fock contribution is explicitly evaluated for each size of the cluster. The dimer correlation energy is however assumed to be transferable in the cluster within an additive pairwise scheme. In the present model, charge transfer may occur in the HF contribution.

2.3 Optimization procedures and Lennard-Jones approximation

In order to save computing time to deduce the ground-state lowest-energy configurations, we proceed as follows. First the simulated annealing technique is used to explore energy surfaces obtained from a crude additive pairwise expression of the energy assuming an approximated Lennard-Jones form of equation (4):

$$E(Ba_n) = \sum_{i<j} \left(\frac{C_{12}}{R_{ij}^{12}} - \frac{C_6}{R_{ij}^6}\right) \cdot \qquad (5)$$

The value $5.5115 \times 10^9\ a_0^{12}$ Hartree for the C_{12} coefficient has been obtained by fitting the dimer data with the previous effective value of C_6 coefficient held fixed. At this step, initial configurations are obtained. Then starting from these geometries, optimizations by gradient techniques are performed using this time energies calculated with the various methods considered in the present work, namely HF+MP2, LSDA and model HF + dispersion calculations through equation (4).

The Lennard-Jones approximation is obviously not so accurate than are calculations such as *ab initio*, HF+pairwise dispersion interaction. In this empirical model, parameters are fitted, once for all, on the ground state potential well of Ba_2. Indeed, this Lennard-Jones approximation is not appropriate to study a non metal-metal transition. Nevertheless, this is a suitable way to determine some not too uncertain geometries to be used as starting point for more accurate calculations. In fact if we compare the results provided by this rather crude approach to those from our more precise calculations, the main difference lies in the evolution of the mean internuclear distance when the cluster size increases. In contrast with the HF+pairwise dispersion interaction, the Lennard Jones potential does not give rise to any contraction of this mean internuclear distance. This statement prevents this model to account for any change in the binding nature when the cluster size increases. Nevertheless actually, the global structure and symmetry remain unchanged.

Concerning the minimization procedure using the simulated annealing algorithm, we generally heat the cluster over the melting temperature of barium bulk (typically 1000 K). Then, the temperature is decreased by step of 20 K. For each step, the number of used configurations is sufficiently large (≈ 100000) in order to try to overfly the complete potential energy surface.

3 Results

3.1 Equilibrium geometries from Ba_2 to Ba_6

The most stable geometrical structures obtained from Ba_2 to Ba_6 through the minimization of LSDA energies with an analytical gradient procedure are drawn in Figure 1 while some isomer configurations with higher energies are displayed in Figure 2. The corresponding positions of the atoms are presented in Table 2 following the notations of Montag and Reinhard (MR) [4], adapted to the classification of axially symmetric structures (z and ρ are the coordinates of the atoms on the various rings). Dissociation energies,

$$E_n^{diss}(1) = E(Ba_n) - E(Ba_{n-1}) - E(Ba) \qquad (6)$$

are also reported in Table 2 as well as the difference between the energy of the most stable structure and that of the second isomer.

The ground state of Ba_2 was investigated previously in a rather elaborated MRCI scheme [11] and the corresponding results are considered here as a reference. Comparison with the present LSDA and MP2 calculations point

Table 2. Stable structures (in the notation from [4]) of Ba_n clusters deduced from various type of calculations. A great number of clusters is axially symmetric. In this notation z is the symmetry axis, z_i (a.u.) is the distance from $z = 0$, and ρ_i (a.u.) is the radius of the circle. On this circle, n atoms are placed with an angle $2\pi/n$.

		Present calculations															
		Model				DFT(LSDA)				HF+MP2				Montag *et al.* [4] results			
Struc.	Sym.	Coordinates z_j/ρ_i			E(eV)	Coordinates z_j/ρ_i			E(eV)	Coordinates z_j/ρ_i			E(eV)	Coordinates z_j/ρ_i			E(eV)
		1	2	3	(ΔE)	1	2	3	(ΔE)	1	2	3	(ΔE)	1	2	3	(ΔE)
Ba_2	{11}	$D_{\infty h}$	4.75	$-z_1$	0.16	4.84	$-z_1$		0.24	5.41	$-z_1$		0.09	4.55	$-z_1$		
			0.0	0.0		0.0	0.0			0.0	0.0			0.0	0.0		
Ba_3	{3}	D_{3h}	0.0		0.45	0.0			0.59	0.0			0.25	0.0			
			5.23			5.32				5.72				4.3			
	{3}	$D_{\infty h}$	9.32	0.0	$-z_1$	(−0.25)				10.6	0.0	$-z_1$	(−0.16)	6.6	0.0	$-z_1$	(−0.54)
			0.0	0.0	0.0					0.0	0.0	0.0		0.0	0.0	0.0	
Ba_4	{13}	T_d	7.15	0.0		(0.85)	7.34	0.0		0.99	7.63	0.0		0.63	6.0	0.0		
			0.0	5.06			0.0	5.19			0.0	5.39			0.0	4.3		
Ba_5	{131}	D_{3h}	7.4	0.0	$-z_1$	0.77	7.58	0.0	$-z_1$	0.78	7.98	0.0	$-z_1$	0.40	7.0	0.0	$-z_1$	
			0.0	4.9	0.0		0.0	5.08	0.0		0.0	5.16	0.0		0.0	4.3	0.0	
	{14}	C_{4v}													4.2	−1.0		(−1.01)
															0.0	5.6		
Ba_6	{222}	C_{2v}	2.41	0.0	−5.98	0.86	1.22	0.0	−6.92	0.84	2.79	0.0	−6.63	0.51				
			7.34	4.11	4.51		7.74	4.31	4.45		7.89	4.39	4.94					
	{141}	D_{4h}	6.23	0.0	$-z_1$	(−0.26)									4.5	0.0	$-z_1$	
			0.0	6.24	0.0										0.0	6.1	0.0	

			$E_{\rm HF} - \sum_{i>j} \frac{C_6 f_6(R_{ij})}{R_{ij}^6}$								Montag *et al.*			
Struc.		Sym.	Coordinates(z_j/ρ_i)						E(eV)		Coordinates(z_j/ρ_i)			E(eV)
			1	2	3				(ΔE)		1	2	3	(ΔE)
Ba_7	{151}	D_{5h}	4.0	0.0	$-z_1$				1.21		3.6	0.0	$-z_1$	
			0.0	7.55	0.0						0.0	7.0	0.0	
		C_{3v}	4.72	0.0	−1.84				(−0.24)		6.2	0.0	−2.8	(−1.05)
			4.98	8.41	0.0						0.0	4.3	4.3	
Ba_8	$\{1515_1\}$	—	see Table 3						1.06					
	{161}	D_{6h}	3.91	0.0	$-z_1$				-(0.75)		3.7	0.0	$-z_1$	
			0.0	8.29	0.0						0.0	7.4	0.0	
	{2222}	C_{2v}	0.0	4.68	8.33	13.75			(−0.26)					
			4.28	6.35	4.10	4.73								
Ba_9	$\{16_422\}$	—	see Table 3						1.38					
	{12222}	C_{2v}	-7.26	-2.08	0.0	5.94	7.57		(−0.16)					
			0.0	7.09	3.93	4.07	7.73							
Ba_{10}	{3313}	C_{3v}	-5.91	−1.05	0.0	2.87			1.51					
			5.01	7.85	0.0	7.29								
	{122221}	D_{2h}	10.25	4.84	2.96	$-z_3$	$-z_2$	$-z_1$	(−0.26)					
			0.0	7.06	3.96	ρ_3	ρ_2	0.0						
Ba_{11}	$\{216_422\}$	—	see Table 3						1.61					
		—	see Table 3											
Ba_{12}	{22422}	D_{2h}	-5.15	-2.59	0.0	$-z_2$	$-z_1$		1.76					
			6.49	4.08	10.0	ρ_2	ρ_1	0.0						
Ba_{13}	{15151}	D_{5h}	-7.97	-3.57	0.0	$-z_2$	$-z_1$		2.21					
			0.0	7.13	0.0	ρ_2	ρ_1	0.0						
Ba_{14}	{331331}	C_{3v}	-6.22	−1.31	0.0	1.55	6.39	13.17	1.48					
			4.85	7.77	0.0	7.77	4.63	0.0						

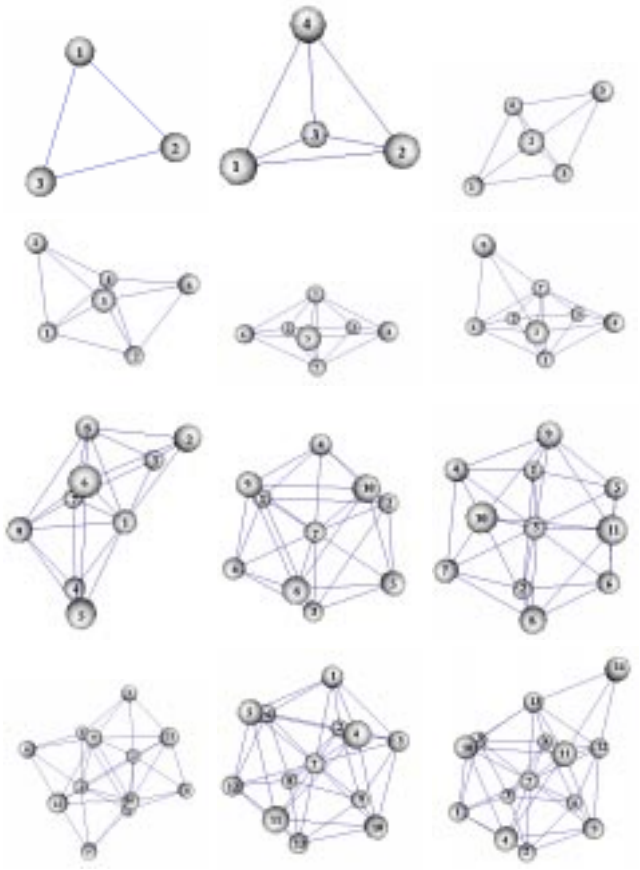

Fig. 1. Lowest-energy ground state isomers of Ba_n clusters ($n = 3$, 14).

Fig. 2. Some isomer configurations of Ba_n clusters ($n = 3$, 11).

out that LSDA results appear to be in better agreement with reference data than MP2 ones, showing a relative difference of $\approx 5\%$ for the equilibrium distance R_e and of $\approx 15\%$ for the dissociation energy. A good agreement is also obtained for the value of the harmonic frequency $\omega_e = 37$ cm^{-1} with a difference of 2 cm^{-1}. The larger binding energy obtained with LSDA may confirm previous remarks about the adequacy of LSDA methods to treat alkaline earth dimers [15]. Due in large part to some lack of correlation effects, MP2 results are too large for the equilibrium distance and too small as concerns the dissociation energy.

For all clusters Ba_n in the range $n = 3-6$, identical equilibrium geometrical structures have been obtained either with the MP2 or LSDA methods as well as with the model calculations. They differ only in the values of the interatomic distances. The lowest-energy configurations are an equilateral triangle for Ba_3, a regular tetrahedron for Ba_4 and a trigonal bipyramid for Ba_5. Similar ground state geometries were obtained for Be_n [5] and Mg_n [6] clusters in this small size range. From Ba_3 to Ba_5 the relative difference in the geometric parameters calculated at the MP2 and at the LSDA levels respectively remains smaller than 5% with systematically higher values obtained in the MP2 approximation.

The only previous calculations we knew for the ground state structure of barium clusters are due to Onwuagba (1993) [3] and to Montag and Reinhard (1995) [4]. Onwuagba investigated properties of barium clusters in the Jellium model using the spin-polarized local density approximation in the framework of density functional theory. Montag and Reinhard used the Cylindrically Averaged Pseudopotential method CAPS. The CAPS method also belongs to the density fonctional theory approach and the Kohn-Sham description of the valence electrons, but uses explicit electron-ion pseudopotentials which are cylindrically averaged, thus introducing an axial constraint. Their results are quoted in Table 2 for comparison. First it should be noted that the equilibrium geometries derived in the present three-dimensional approach are the same as those obtained in CAPS for Ba_3, Ba_4 and Ba_5. For these small clusters the relative differences in the geometric parameters are within 8−18% with systematically smaller values in CAPS calculations. A larger difference is obtained for the distance between two consecutive Ba atoms in the linear Ba_3 isomer. When compared to the equilibrium distance $R_e(Ba_2)$ for the dimer, a rather large reduction ($\approx 28\%$) is found in CAPS results while the Ba_2 distance in Ba_3 obtained here is nearly equal to that of the isolated Ba_2 molecule. Note for instance that Kumar and Car [6], using the local density molecular dynamics method and simulated annealing techniques found a slight reduction of $\approx 3\%$ for the distances in Mg_3 with respect to free Mg_2.

We now examine the equilibrium geometry of Ba_6. For the three determinations of the energy (MP2, LSDA or model) the gradient minimization always leads to a most stable structure {222} with C_{2v} symmetry, contrarily to the previous CAPS results. CAPS calculations predict a

pentagonal pyramid structure {15} (C_{5v} symmetry) to have the lowest energy. It should be noted that we failed in searching such a stable structure. In fact starting explicitly from a pentagonal pyramid geometry, the optimization process was always seen to yield again the {222} lowest-energy stable configuration. In the same way, we did not find structure {222} of MR with D_{2h} symmetry as a stable one. The regular octahedron structure {141} corresponding to D_{4h} symmetry is found to be a stable configuration higher in energy than the structural ground state by an amount of 0.26 eV in the present work and by an amount of 0.6 eV in CAPS calculations. Thus this symmetric configuration is not the lowest-energy one for Ba_6 contrarily to rare gas hexamers. In fact this result is similar to that obtained for Mg_6 [6].

Thus there seem to be differences in the building of Ba_n clusters with respect in particular to Be_n clusters. One should recall than the binding in Be_2, a former challenge for Quantum Chemistry, is a very peculiar one, with short molecular distance, and larger dissociation energy that usual for Van der Waals dimers. This is due to a strong participation of p^2 atomic character in the molecular wavefunction and is significantly different from Mg_2 and Ba_2 which remain essentially Van der Waals dimers (weak D_e value and large R_e value with respect to the atomic radii). This qualitative difference in the binding character, already present on the dimer, seems to extend to large clusters in the size range of interest here.

Because present model calculations are independent from LSDA results, quantitative comparisons between the two sets of values are meaningful. As a matter of fact, the geometric parameters obtained with LSDA and with our model calculations respectively, agree quite well for the stable structures from Ba_2 to Ba_6 with relative differences smaller than 7%, including the linear structure of the Ba_3 isomer. The agreement is also reasonable for the dissociation energies.

The adequacy of the present model to calculate the total energy of Ba_n in this range is to some extent also ascertained by the analysis of the electronic density maps from Ba_3 to Ba_5. The differences $\delta\rho$ between molecular and atomic electronic densities have been calculated with the CIPSI wavefunctions as described in Section 2, using the geometric parameters which minimize the LSDA energies for Ba_3, Ba_4 and Ba_5 respectively. The various $\delta\rho$ maps are drawn in Figure 3 for Ba_3 (a), Ba_4 (b and c) and Ba_5 (d). In the case of Ba_2 a weak binding obtained at the HF level (not an artefact of BSSE) and a noticeable increase of the electronic density betwen the atoms, indicate a slight deviation from pure Van der Waals character, however not comparable with the Be_2 case. For Ba_3 and Ba_4 the binding character is similar to that seen for Ba_2.

Then the energy of small Ba_n clusters may be calculated with an expected reasonable accuracy through a two-body type model.

3.2 Equilibrium geometries from Ba_7 to Ba_{14}

Only model calculations have been performed for the energy (Eq. (3)) of these clusters due to computational capability constraints. This model having provided results in quite good agreement with those obtained from LSDA for the smallest clusters Ba_n ($n = 2-6$), we expect reliable results for the largest ones in the range $n = 7-14$ as long as no strong transition to metallic character occurs, in which case the model calculation of the correlation energy would somewhat break down. To ascertain this assumption we have also performed LSDA calculation for Ba_9. Stable geometrical configurations have been obtained using a numerical gradient procedure after a first search with simulated annealing techniques as described in Section 2.3. The lowest-energy structures are drawn in Figure 1 while some isomer configurations are drawn in Figure 2. The corresponding geometrical parameters and dissociation energies are reported in Table 2 for axially symmetric clusters. For the three clusters Ba_8, Ba_9 and Ba_{11} we report bond lengths, dissociation energies and isomer energies in Table 2.

For Ba_7, a pentagonal bipyramid {151} structure with D_{5h} symmetry occurs to be the lowest-energy isomer as predicted in the CAPS calculations of Montag and Reinhard [4]. It may be built by capping three faces of the Ba_4 tetrahedron. An isomer lying ≈ 0.23 eV above this pentagonal bipyramid is also stable. Its geometry corresponds to structure {133} with C_{3v} symmetry and can be built either by capping two adjacent faces of the trigonal bipyramid isomer of Ba_5 or by capping the 1-3-2 face (see Fig. 2) of the lowest-energy configuration of Ba_6. Similar results have been predicted for Mg_7 [6].

The most stable isomer obtained for Ba_8, not axially symmetric, can be built up by capping one face of the pentagonal bipyramid Ba_7, similarly to previous findings for the Mg_8 cluster [6]. This result differs from the CAPS predictions. As a matter of fact, structure {161} with D_{6h} symmetry, predicted as the lowest-energy one in CAPS, is found here to correspond to an isomer lying ≈ 0.74 eV higher in energy. A more stable isomer lying ≈ 0.25 eV higher above the lowest one is also predicted. It corresponds to a {2222} structure with C_{2v} symmetry.

The minimum energy structures derived here for Ba_n clusters are different from the CAPS calculations of MR for $n = 9$ and 10. They also differ from results concerning Be_n [5] and Mg_n [6]. For beryllium and magnesium clusters, the authors [5,6] have performed calculations using a Density Functionnal Molecular Dynamics procedure (DFT-MD). The approximation used for the energy calculation (LSDA) is the same than in our case which makes fully valuable the comparison between their results and ours. For Ba_9 the lowest-energy isomer has C_{2v} symmetry and can be built up by capping two adjacent faces of the slightly distorted Ba_7 bipyramid. It differs from the {144} structure with C_{2v} symmetry predicted in CAPS as well as from the tricapped trigonal prism geometry derived for Mg_9 [6] or for Be_9 [5].

We also obtain an isomer corresponding to a {12222} structure with C_{2v} symmetry 0.15 eV above the

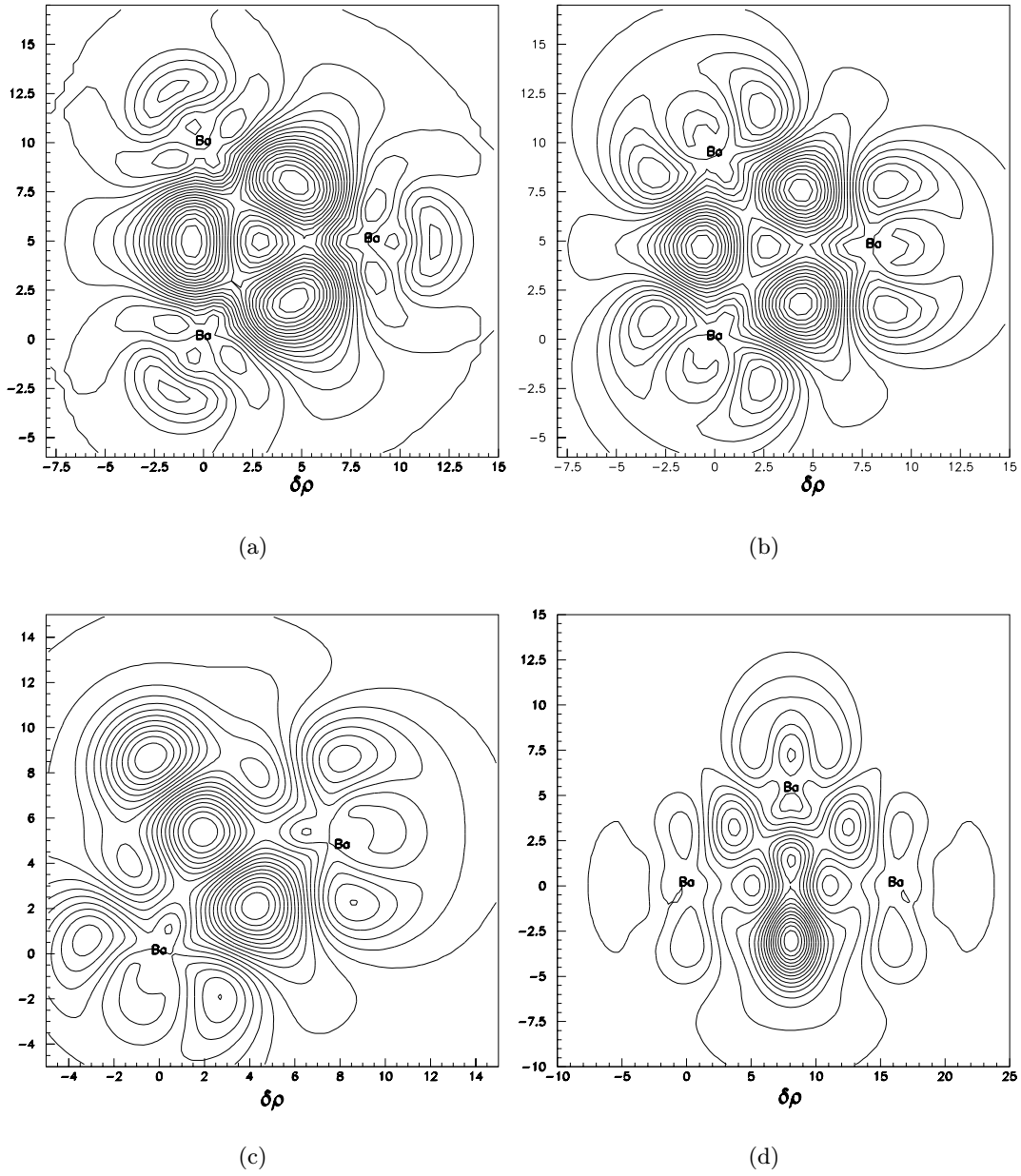

Fig. 3. Differential density maps for Ba_n. (a) Ba_3; (b) Ba_4 in the plane of the triangular basis defined by the atoms 1, 2, 3 (see Fig. 1); (c) Ba_4 in the plane containing atoms 1 and 2 and perpendicular to the axis 3–4; (d) Ba_5 in the plane containing atoms 1, 2, 5 and perpendicular to the axis 3−4.

lowest-one. It may be formed by capping two opposite faces of a distorted pentagonal bipyramid. Because $n = 9$ is the first size for which the most stable structures found here are different from those of MR on Ba_9, and also from those of Mg_n [6] and Be_n clusters [5] and in order to check that this difference is not due to use of the present model, we have also performed LSDA calculations using the basis set previously used for $n = 2-6$. Both geometries, namely the C_{2v} one (bicapped pentagonal bipyramid) and the C_{3v} (tricapped trigonal prism) predicted by Kumar and Car [6] for Mg_9 have been investigated. Minimization has been performed with gradient techniques. LSDA calculations confirm that for Ba_9 the C_{2v} isomer is lower in energy than the C_{3v} one by an amount of ≈ 1 eV. The most stable structure obtained for Ba_{10} has {3313} structure with C_{3v} symmetry. It differs from the {1441} structure with D_{4d} symmetry predicted in CAPS for Ba_{10} as well as from that of Be_{10} [5]. An isomer structure {122221} with symmetry D_{2h} is obtained 0.25 eV higher in energy. It may be obtained by capping one edge of the C_{2v}{12222} isomer of Ba_9.

The minimum energy structure predicted for Ba_{11} has C_{2v} symmetry and corresponds to a tetracapped pentagonal bipyramid. We also find an isomer which consists in

Table 2. Bond lengths for Ba_8, Ba_9 and Ba_{11} clusters. The labelling of atoms is displayed in Figure 1.

Cluster	Bond	R (a.u.)
Ba_8	1-2=1-3=1-4=1-5=1-6=2-7=3-7=4-7=5-7=6-7	8.57
	1-7	8.00
	2-3=2-6=3-4=4-5=5-6	8.91
	2-4=2-5=3-5=3-6=4-6	14.42
	6-8=5-8=7-8=4-8=2-8	14.23
	1-8	14.00
	7-8	8.34
	6-8=5-8	8.72
	3-8	16.62
Ba_9	1-2=1-3=1-4=1-5=2-3=4-5	8.14
	1-6=1-7	8.24
	1-8=1-9	7.92
	2-4=3-5	16.28
	2-5=3-4	14.10
	2-6=3-7=4-7=5-6	13.81
	2-7=3-6=4-6=5-7	8.82
	2-9=3-9=4-8=5-8	13.80
	2-8=3-8=4-9=5-9	8.20
	6-8=6-9=7-8=7-9	8.47
	8-9	8.74
	6-7	13.86
Ba_{11}	1-2	11.90
	1-3=2-3	7.85
	1-4=1-5=2-7=2-6	8.86
	1-5=1-6=2-4=2-7	13.20
	1-9=2-8	8.84
	1-8=1-9	15.40
	1-10=1-11=2-10=2-11	13.75
	3-4=3-5=3-6=3-7=4-5=6-7	8.05
	3-8=3-9	7.66
	3-10=3-11	7.78
	4-6=5-7	16.10
	4-5=7-6	13.94
	4-9=5-9=7-8=6-8	8.28
	4-8=5-8=6-9=7-9	13.35
	4-10=7-10=6-11=5-11	8.15
	4-11=7-11=6-10=5-10	13.58
	8-9	13.64
	8-10=8-11=9-10=9-11	8.59
	10-11	8.46

the addition of one atom to the C_{2v} {122221} isomer of Ba_{10} and which lies ≈ 0.31 eV above the lowest configuration. The most stable structure for Ba_{12} is found to be {1515} with D_{5h} symmetry. We also predict an isomer corresponding to a {22422} structure with symmetry D_{2h} in which a pentagonal bipyramid can be clearly identified.

The lowest-energy configuration of Ba_{13} is found to be a regular icosahedron, corresponding to {15151} structure with D_{5h} symmetry, as often found for 13-atom clusters, especially Lennard-Jones clusters. It should be noted that this prediction is consistent with experimental observations on Ba_n clusters produced by the inert-gas condensation technique [1] where the magic sizes 13, 19, 23... characteristic of icosahedral structures were seen to be the most abundant.

Ba_{14} is found to have a {331331} structure with C_{3v} symmetry which can be described as an icosahedron with one capping atom. To the best of our knowledge there exist no previous structural results from Ba_{11} to Ba_{14}.

The growth behavior from Ba_7 to Ba_{13} appears to be characterized by the addition of atoms around a pentagonal bipyramid. It is different from the mechanism of prism addition and rhombus capping obtained for the growth of Be clusters for $n \geq 7$. It also differs from the growth behavior of Mg clusters in which a tetrahedron and a trigonal prism were found to be important building constituants. This different growth mechanism for Ba_n results in the icosahedral structure for Ba_{13} unlike the lowest-energy configuration derived for Be_{13} and for Mg_{13}. Indeed, fundamental differences appear between the growth sequence of different alkaline-earth metals in the range

$6 \leq n \leq 9$: typically, a 5-folding symmetry skeleton for Ba_n and hexagonal symmetry for Be_n and Mg_n. This is consistent with the bulk lattice structure: compact hexagonal for beryllium and magnesium, bcc for barium.

3.3 Stability and abundance of Ba_n clusters n = 2, 14

In order to examine characteristics in the total energy for specific cluster sizes, one generally defines as a measure of the relative stability the following quantity,

$$\Delta_2(n) = E_{n+1} - 2E_n + E_{n-1} \tag{7}$$

related to the second derivative of the energy with respect to n. It is shown in Figure 4b that the 4-, 7- and 13-atom clusters correspond to maxima in $\Delta_2(n)$ and that they may be considered as relatively stable. This is also corroborated by the variation with cluster size of the dissociation energy $E_n^{\rm diss}(1)$ previously defined (Eq. (6)) and generalized as

$$E_n^{\rm diss}(m) = E(n-m) + E(m) - E(n) \tag{8}$$

which is displayed in Figure 4a for $m = 1$ and 2. $E_n^{\rm diss}(m)$ represent the energy required to break a cluster of size $(n + m)$ into two clusters of size n and m respectively. Maxima in $E_n^{\rm diss}(1)$ are obtained for clusters with 4, 7 and 13 atoms. It should be noted that the energy required to evaporate a dimer is by far larger than that needed for evaporating a single Ba atom. An equivalent measure of the relative stability is obtained by considering the chemisorption of Ba atoms on Ba_n clusters through the chemisorption energy defined as [6]

$$E^{\rm chem}(n) = |E(n+1) - E(n) - E(1)|. \tag{9}$$

$E^{\rm chem}(n)$ is seen Figure 4c to be relatively larger for clusters with 3, 6 and 12 atoms *i.e.* clusters for which adding one atom provides a relatively stable cluster.

From these energetical considerations it may be inferred that Ba_n clusters with $n = 4$, 7 and 13 should be abundant in the mass spectrum. Thus, the present results support only partially the general predictions of jellium-like models. The 4-atom cluster has 8 valence electrons and corresponds to a filled shell in the spherical jellium model [16]. Clusters with 7 and 13 atoms which have 14 and 26 valence electrons respectively correspond to the filling of subshells as predicted by the spheroidal jellium model [17]. However, Ba_{10} which has 20 valence electrons and corresponds to a filled shell in the spherical jellium model is not found to be particularly stable, *i.e.* is not a magic cluster. In fact, the relative stabilities predicted for small Ba_n clusters, may be rather interpreted as due to geometrical effects as observed for clusters where the mechanism consists in the growth of shells of atoms. This corresponds to addition of atoms around the three compact structures, namely the regular tetrahedron, the pentagonal bipyramid and the icosahedron.

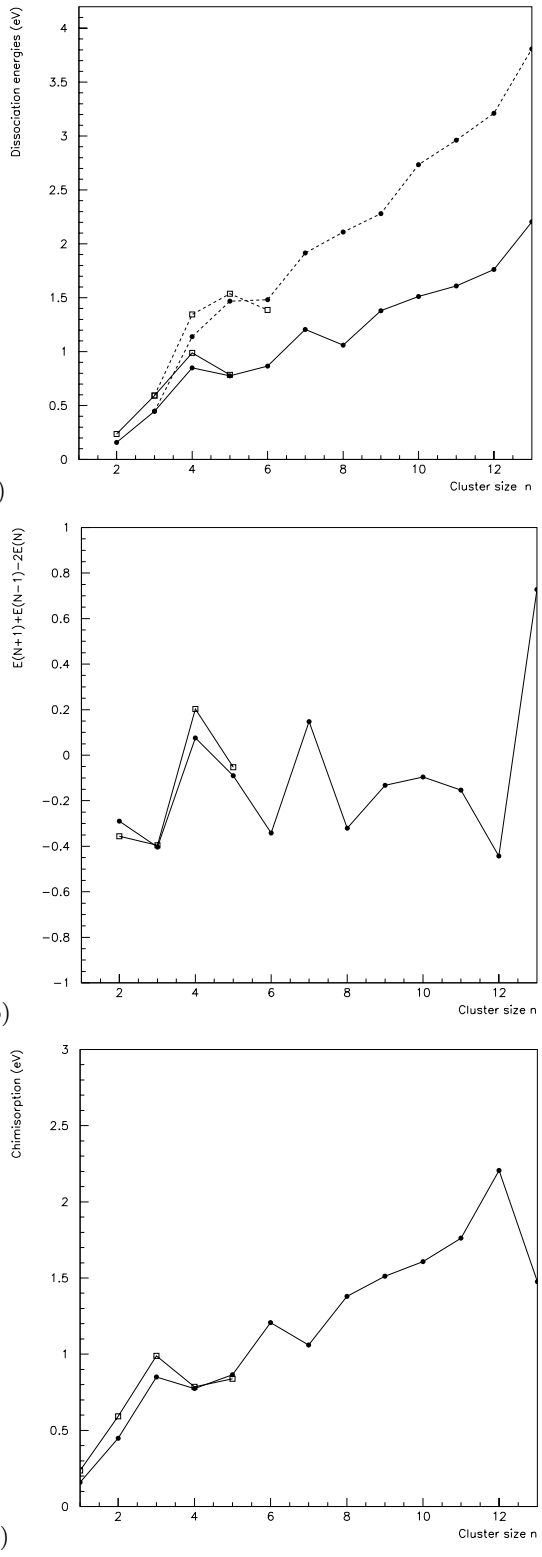

Fig. 4. (a) Dissociation energy: for the monomer $E_n^{\rm diss}(1)$ (full lines), for the dimer $E_n^{\rm diss}(2)$ (dashed lines), (b) second derivative $\Delta_2(n)$ and (c) chemisorption energy $E_n^{\rm chem}(1)$. Squares represent values from LSDA calculations while circles represent values from HF + dispersion model calculations.

Table 3. Vertical ionization potentials (IP) (in eV) of Ba_n clusters ($n = 2-5$). The theoretical IP's are the QCISD(T) values calculated for the geometries deduced from the HF + dispersion model.

Cluster	Experiment	theory
Ba_2	4.23(0.05)	4.13 (4.27 for full CI)
Ba_3	4.1	4.12
Ba_4	4.0	4.06
Ba_5	3.61	3.67

3.4 Ionization potentials

Ionization potentials IP(Ba_n) have been calculated for Ba_2 to Ba_5 clusters in the QCISD(T) *ab initio* scheme described in Section 1 at the geometries of neutrals previously optimized using the model energy (Eq. (4)). Identical geometries are considered for both neutral Ba_n and ionic Ba_n^+ clusters so that vertical ionization potentials are calculated. Results are presented in Table 3 and compared with recent experimental values obtained in our laboratory. We also include the MRCI theoretical value of 4.27 eV for the adiabatic ionization potential of Ba_2 [11].

For Ba_2, the present IP values are seen to be slightly smaller than both our previous result of 4.27 eV and the experimental range values 4.21−4.25 eV [2], with a relative difference smaller than 4%.

From Ba_3 to Ba_5 our results are seen to be in good agreement with the experimental values with a relative difference $\approx 2\%$. While the calculated IP(Ba_3) and IP(Ba_4) are very similar (≈ 4 eV) a significant decrease (≈ 0.4 eV, $\approx 11\%$) is predicted for Ba_5. It should be noted that this is in total agreement with experimental observations. Such a variation may be understood from the relatively larger stability of the Ba_4. This stability is consistent both with geometric criterions, since Ba_4 is a regular tetrahedron and with the spherical jellium model, since it achieves an electronic shell closure at eight valence electrons. With respect to the latter criterion, Ba_5 comparatively has an "excess" of two valence electrons. This is also consistent with the weak, however perceptible, delocalization of the charge density off the bonds when going from Ba_4 to Ba_5 as may be seen in Figure 3.

3.5 Discussion and conclusion

We have investigated the structure and growth behavior of Ba_n clusters up to 14 atoms without any symmetry constraints. For the small sizes, the present results are consistent with those obtained in the CAPS scheme. In the case of intermediate sizes ($n = 8-10$) differences do occur, may be due to the cylindrical constraint affecting the CAPS results. For $n > 8$, the lowest-energy isomers are different from those previously predicted for Be_n and Mg_n clusters. In the range 8−14, the growth pattern appears to be different from that of Be_n and Mg_n, and is governed by pentagonal bipyramid capping. This leads to the icosahedral structure obtained for Ba_{13} in consistency

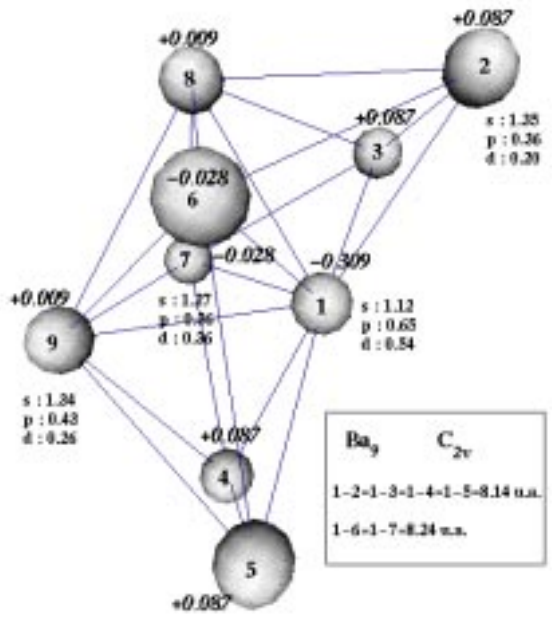

Fig. 5. Estimated LSDA atomic gross population for Ba_9. Value in itallic represent the mean natural charge on each site. "s p d" are related to the mean character of the 2 valence electrons on each barium site.

with the observed size distribution of barium clusters produced by inert-gas condensation techniques.

Density maps displayed in Figure 3 for Ba_3, Ba_4 and Ba_5 illustrate the binding nature in these small clusters. For the 3- and 4-atom clusters the density is similar to that in Ba_2. This remains mainly true for Ba_5 nevertheless a weak delocalization of the density off the bonds is observed. Up to Ba_7, the cluster energies appear to result essentially from the addition of pair contributions. For larger sizes, the structures appear to remain similar to that for Lennard-Jones type clusters while slight modifications in terms of Mulliken population become noticeable as seen from our calculation on Ba_9. From LSDA calculations we have estimated the gross orbital populations for each of the 9 atoms. The results are presented in Figure 5 for the atoms labelled 1, 2 (equivalent to 3, 4 and 5), 7 (equivalent to 6) and 9 (equivalent to 8). The averaged population over the nine atoms is $\approx 65\%$ in s orbitals, $\approx 20\%$ in p orbitals and $\approx 15\%$ in d orbitals, showing that the bonding appears to remain mainly due to s electrons. Nevertheless the populations on atom 1 (with coordination 6) are significantly different from those calculated for the other atoms. The influence of p (28%) and d (23%) orbitals is somewhat larger. Furthermore an atomic charge of -0.308 is estimated for this atom, showing some beginning trend to charge transfer along the bonds of atom 1 with its 6 nearest neighbours (with weak positive charges).

Additional information related to the departure from non metal structure can be deduced from the cohesive energy per atom. In Figure 6, our calculated values are compared to both Van der Waals structures (normalized to the Van der Waals energy in the bulk) [18] and

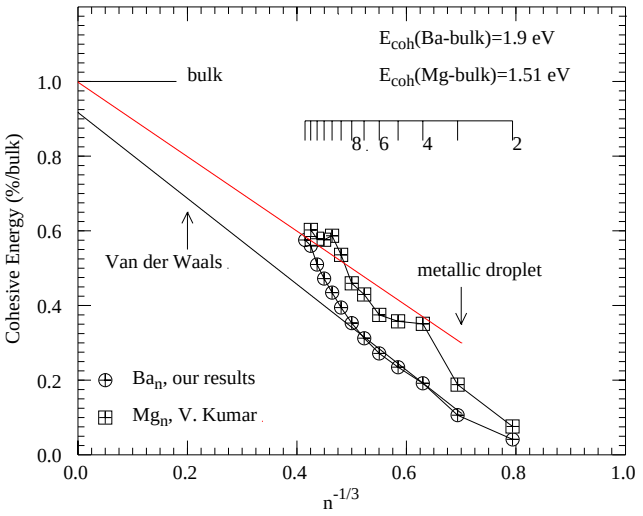

Fig. 6. Comparison of the cohesive energy per atom for barium clusters (HF + pair dispersion) and magnesium clusters (Kumar *et al.* [6]) with both pure Lennard-Jones calculations and the liquid droplet model. In order to compare the behavior of the curves for Ba_n and Mg_n clusters, values have been normalized to the bulk cohesive energy.

metallic droplet for which the cohesive energy is given by $5/8e^2/R_s n^{1/3} + W_0$, where $W_0 = 2.49$ eV is the work function of the bulk and n the number of atoms in the cluster, for barium. It appears very clearly that a deviation from the initial Van der Waals cohesive energy starts at $n = 5{-}6$. While the calculated values evolve regularly towards the metallic droplet curve, we can only underline this tendency. Indeed, the lack of calculated values for larger clusters prevented us to ascertain whether beyond $n = 14$ the cohesive energy per atom is well represented by the metallic droplet model. This model was very succesfull to demonstrate the metallic character of large sodium [19] and mercury [20,21] clusters. In Figure 6, one can notice for small Mg_n clusters that the cohesive energy exhibits the same behaviour as the present values for calculated Ba_n clusters (departure from the Van der Waals binding). Nevertheless for Hg_n clusters cohesive energy deduced from previous experiments [20] gave results up to some hundreds atoms and it appears that a metallic character is established only close to $n = 100$. It is also worthwhile to notice the thermodynamical approach of divalent structures by Miedema [22]. By comparison of the free enthalpy of vaporization and electron promotion from s to p orbitals, the author concluded that, in so far as alkaline earth structures are concerned, only the dimer should have Van der Waals binding.

In conclusion, our results, consistent with those former works, emphasize some different aspects (electron delocalization, charge transfer, cohesive energy per atom) which can be considered as possible indications, on the molecular scale, of the beginning of a non metal-metal transition. Ionization potential measurements for larger clusters would be of great interest to check this transition and determine a possible critical size for the metallic behaviour. Moreover, the calculated growth sequence of barium clusters seems different from lighter alkaline earth metals and leads to the compact icosahedral structure.

Further fully *ab initio* confirmations will be necessary to ascertain the results beyond $n = 9$, explicitly taking into account the influence of s-p hybridization and consistent correlation. Even for smaller sizes, evaluations of the accuracy of the LSDA approximation with respect to more sophisticated functional expressions or to size-consistent CI type calculations are needed.

References

1. D. Rayane, P. Melinon, B. Cabaud, A. Hoareau, B. Tribollet, M. Broyer, Phys. Rev. A **39**, 6056 (1989).
2. V. Boutou, M.A. Lebeault-Dorget, A.R. Allouche, C. Bordas, J. Chevaleyre, Z. Phys. D **40**, 448 (1997).
3. B.N. Onwuagba, Phys. Stat. Sol. (b) **180**, 391 (1993).
4. B. Montag, P.G. Reinhard, Z. Phys. D **33**, 265 (1995).
5. R. Kawai, J.H. Weare, Phys. Rev. Lett. **65**, 80 (1990).
6. V. Kumar, R. Car, Phys. Rev. B **44**, 8243 (1991).
7. U. Rothlisberger, W. Andreoni, P. Giannozzi, J. Chem. Phys. **96**, 1248 (1992).
8. P. Fuentealba, O. Reyes, H. Stoll, H. Preuss, J. Chem. Phys. **87**, 5338 (1987).
9. B. Huron, P. Rancurel, J.P. Malrieu, J. Chem. Phys **58**, 5475 (1973); S. Evangelisti, J.P. Daudey, J.P. Malrieu, Chem. Phys. **75**, 95 (1983).
10. M.J. Frisch, G.W. Trucks, H.B. Schlegel, P.M.W. Gill, B.G. Johnson, M.A. Robb, J.R. Cheeseman, T. Keith, G.A. Petersson, J.A. Montgomery, K. Raghavachari, M.A. Al-Laham, V.G. Zakrzewski, J.V. Ortiz, J.B. Foresman, C.Y. Peng, P.Y. Ayala, W. Chen, M.W. Wong, J.L. Andres, E.S. Replogle, R. Gomperts, R. L. Martin, D.J. Fox, J.S. Binkley, D.J. Defrees, J. Baker, J.P. Stewart, M. Head-Gordon, C. Gonzalez, J.A. Pople, Gaussian 94, Revision B.3, Gaussian, Inc. (Pittsburgh PA, 1995).
11. A.R. Allouche, M. Aubert-Frécon, G. Nicolas, F. Spiegelmann, Chem. Phys. **200**, 63 (1995).
12. A. Karo, M. Krauss, A.C. Wahl, Int. J. Quantum Chem. Quantum Chem. Symp. **7**, 143 (1973).
13. K.T. Tang, J.P. Toennies, C.L. Yiu, Phys. Rev. Lett. **74**, 1546 (1995).
14. L.N. Shabanova, Opt. Spectry **27**, 205 (1969).
15. G. Ortiz, P. Ballone, Phys. Rev. B **43**, 6376 (1991).
16. W.D. Knight, K. Clemenger, W.A. de Heer, W.A. Saunders, M.Y. Chou, M.L. Cohen, Phys. Rev. Lett. **52**, 2141 (1984).
17. K. Clemenger, Phys. Rev. B **32**, 1359 (1985).
18. B. Van de Waal, J. Chem. Phys. **90**, 3407 (1989).
19. C. Bréchignac, H. Busch, Ph. Cahuzac, J. Leygnier, J. Chem. Phys. **101**, 6992 (1994).
20. H. Haberland, H. Langhosch, Z. Phyz. D **19**, 223 (1991).
21. K. Rademann, B. Kaiser, U. Even, F. Hensel, Phys. Rev. Lett. **59**, 2319 (1987). K. Rademann, J. Phys. Chem. **93**, 653 (1989).
22. A.R. Miedema, J.W.F. Dorleijn, Phil. Mag. B **43**, 251 (1981).